



On crystallization and oxidation behavior of $Zr_{54}Cu_{46}$ and $Zr_{27}Hf_{27}Cu_{46}$ thin-film metallic glasses compared to a crystalline $Zr_{54}Cu_{46}$ thin-film alloy

M. Kotrlová, P. Zeman*, Š. Zuzjaková, M. Zítek

Department of Physics and NTIS – European Centre of Excellence, University of West Bohemia, Univerzitní 8, 306 14 Plzeň, Czech Republic

ARTICLE INFO

Keywords:

Zr–Cu
Zr–Hf–Cu
Metallic glass
Crystallization kinetics
Oxidation kinetics
Activation energy

ABSTRACT

Amorphous $Zr_{54}Cu_{46}$ and $Zr_{27}Hf_{27}Cu_{46}$ thin-film metallic glasses were prepared by non-reactive magnetron co-sputtering of Zr, Hf and Cu in pure argon. Several as-deposited $Zr_{54}Cu_{46}$ films were post-annealed in high vacuum to create a crystalline thin-film alloy of the identical composition. The non-isothermal crystallization behavior of the amorphous $Zr_{54}Cu_{46}$ and $Zr_{27}Hf_{27}Cu_{46}$ films and the effect of a substitution of Hf for Zr on the crystallization process were studied by differential scanning calorimetry. The activation energy of the crystallization was obtained by the Kissinger–Akahira–Sunose method. The results show that the activation energy of the $Zr_{27}Hf_{27}Cu_{46}$ film was higher for all conversion fractions, which indicates that the substitution of Hf for Zr enhances the thermal stability of the glassy state. Considerable attention was also paid to the isothermal oxidation behavior of the amorphous and crystalline $Zr_{54}Cu_{46}$, and amorphous $Zr_{27}Hf_{27}Cu_{46}$ films investigated by thermogravimetric analysis. It was shown that all oxidation curves in the temperature range from 400 to 575 °C obeyed the parabolic law. The activation energy of the oxidation process determined by the Arrhenius equation for the oxidation rate constants was found to be the highest for the $Zr_{27}Hf_{27}Cu_{46}$ film, which indicates that its surface oxide layer is a more effective barrier against the diffusion of species.

1. Introduction

Metallic glasses have attracted considerable interest in recent years due to their unique properties such as high tensile strength, high elastic strain and hardness, temperature-independent electrical resistivity, low wear and high corrosion resistance, excellent surface finishing, and biocompatibility [1–3]. Metallic glasses are amorphous materials with a short-range order on the atomic scale, which gives rise to some specific properties such as homogeneity, isotropy, and absence of grain boundaries [4,5] compared to conventional crystalline materials.

Zr- and Cu-based metallic glasses are one of the most studied systems because of their high crystallization temperature and a wide supercooled liquid region [6,7]. Their unique properties make them attractive for miscellaneous applications. An important prerequisite to use them in industry is their ability to resist an oxidizing environment at elevated temperatures. Recently, several studies have been conducted with the aim to investigate the oxidation behavior and determine the oxidation kinetics of Zr- and Cu-based glassy and/or crystalline thin films [8–12]. To better understand the thermal behavior of the Zr- and Cu-based metallic glasses, several studies have been also focused on the crystallization kinetics, most of them on isothermal [13–15] or a combination of isothermal and non-isothermal kinetics

[16,17] and only a few on non-isothermal kinetics [18–20].

In the present work, thermally activated processes in $Zr_{54}Cu_{46}$ and $Zr_{27}Hf_{27}Cu_{46}$ films prepared by magnetron co-sputtering of Zr, Hf and Cu in argon atmosphere are systematically investigated. We use differential scanning calorimetry to study the non-isothermal crystallization behavior of the amorphous $Zr_{54}Cu_{46}$ and $Zr_{27}Hf_{27}Cu_{46}$ thin-film metallic glasses and to evaluate the influence of a substitution of Hf for Zr on the crystallization process and its activation energy. We pay considerable attention to thermogravimetric analysis of the oxidation behavior of amorphous and crystalline $Zr_{54}Cu_{46}$, and amorphous $Zr_{27}Hf_{27}Cu_{46}$ films. We determine oxidation rate constants and activation energies of the relevant oxidation processes. The selection of the elemental composition of the films investigated was done based on our previous studies [21,22] reporting on properties and thermal behavior of these films.

2. Experimental details

Amorphous $Zr_{54}Cu_{46}$ and $Zr_{27}Hf_{27}Cu_{46}$ thin films were deposited by non-reactive magnetron co-sputtering of Zr (99.5% purity), Hf (99.9% purity) and Cu (99.99% purity) targets in pure argon at a pressure of 0.53 Pa. Magnetrons with the Zr and Hf targets were operated in dc

* Corresponding author.

E-mail address: zemanp@kfy.zcu.cz (P. Zeman).

<https://doi.org/10.1016/j.jnoncrysol.2018.09.004>

Received 13 July 2018; Received in revised form 29 August 2018; Accepted 2 September 2018

0022-3093/ © 2018 Elsevier B.V. All rights reserved.

regimes while the magnetron with the Cu target was operated in a high-power impulse regime. The films were deposited onto Si(100) wafers and molybdenum foils (0.1 mm in thickness) held at a floating potential without any external heating. The substrates were rotated above the targets at a speed of 40 rpm and located at a target-to-substrate distance of 150 mm. More technical details concerning the preparation of Zr–Cu and Zr–Hf–Cu films are given in our previous papers [21,22].

In order to create a $Zr_{54}Cu_{46}$ crystalline alloy film of the identical composition for the comparison study, several as-deposited films were post-annealed at 465 °C (above the crystallization temperature of 422 °C) for 5 min in a high-vacuum chamber (evacuated down to a base pressure of 5×10^{-6} Pa).

The crystallization behavior of the $Zr_{54}Cu_{46}$ and $Zr_{27}Hf_{27}Cu_{46}$ films was investigated by differential scanning calorimetry (DSC) using a Setaram Labsys DSC 1600 system. Approximately 5 μ m thick film deposited onto the molybdenum foil was relatively easily delaminated from this substrate. Obtained freestanding film fragments of a total mass of 5 mg were then inserted into a 100 μ l alumina crucible covered with a lid. An identical uncharged crucible was used as a reference. The DSC measurements were carried out at different heating rates (10, 20, 30 and 40 °C/min) in argon (a flow rate of 1 l/h) in the temperature range from room temperature up to 600 °C. The cooling rate was in all cases the same as the heating rate. Each run was immediately followed by a second run under the same conditions to serve as a baseline. The calorimeter was calibrated by melting of Pb, Zn and Al standards with purity of $99.998 \pm 0.001\%$. After heating, the film fragments were mechanically ground in an agate mortar to provide a fine powder used for X-ray diffraction measurements.

The oxidation behavior of the $Zr_{54}Cu_{46}$ and $Zr_{27}Hf_{27}Cu_{46}$ films with an area of 1×1 cm² was investigated by high-resolution thermogravimetry (TG) using a symmetrical Setaram TAG 2400 system. The TG analysis was carried out in synthetic air (a flow rate of 1 l/h) with dynamical heating in the temperature range from room temperature up to 800 °C and isothermal annealing at various temperatures in the range from 400 °C to 575 °C for 3 h. The heating rate was set to 10 °C/min upon dynamical heating and 50 °C/min before reaching the isothermal temperature. The cooling rate was set to 30 °C/min in both cases. The Si (100) substrates used were coated on one side only. After subtracting the thermogravimetric signal corresponding to oxidation of the uncoated sides, the resulting thermogravimetric curve gives us the thermogravimetric signal of the film only.

The structure of the as-deposited and annealed films on the Si(100) substrate and powdered heated films was characterized by X-ray diffraction (XRD) using a PANalytical X'Pert PRO diffractometer in the Bragg–Brentano configuration using the Cu K_{α} radiation ($\lambda = 0.154187$ nm).

The elemental composition of the as-deposited films on the Si(100) substrate was analyzed by a Hitachi SU-70 scanning electron microscope operated at a primary electron energy of 20 keV using a Thermo Scientific UltraDry energy dispersive spectrometer (EDS). Zr, Hf and Cu standards were used for the quantitative analysis. The error of the elemental analysis was established to be 1 at.%.

The thickness of the surface oxide layer was determined by a J.A. Woollam Co. variable angle spectroscopic ellipsometer. The measurements were performed in the wavelength range from 300 to 2000 nm using angles of incidence of 65°, 70° and 75° in reflection.

3. Results and discussion

The following section is divided into three subsections. The first one characterizes the structure of all three films investigated in this paper. The second one is focused on the non-isothermal crystallization behavior of the $Zr_{54}Cu_{46}$ and $Zr_{27}Hf_{27}Cu_{46}$ thin-film metallic glasses and on the discussion of the influence of a Hf substitution for Zr on the crystallization process. The third one describes the effect of the structure and the elemental composition on the oxidation behavior and kinetics

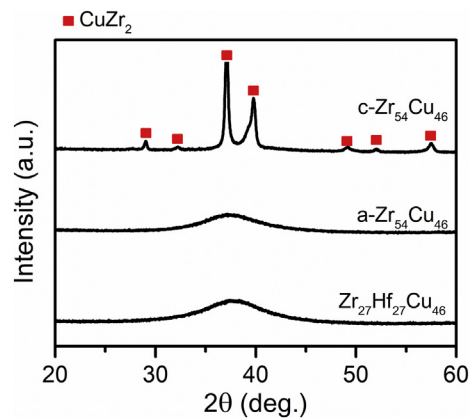


Fig. 1. XRD patterns of as-deposited (a- $Zr_{54}Cu_{46}$ and $Zr_{27}Hf_{27}Cu_{46}$) and annealed (c- $Zr_{54}Cu_{46}$) films.

of the crystalline $Zr_{54}Cu_{46}$ film and amorphous $Zr_{54}Cu_{46}$ and $Zr_{27}Hf_{27}Cu_{46}$ films.

3.1. Structure

XRD patterns of two as-deposited films, $Zr_{54}Cu_{46}$ and $Zr_{27}Hf_{27}Cu_{46}$, and one $Zr_{54}Cu_{46}$ film annealed at 465 °C for 5 min in high vacuum are shown in Fig. 1. It can be seen that the as-deposited films are X-ray amorphous while the annealed film is crystalline. The XRD patterns of the amorphous films contain one very broad peak of a low intensity at the position $2\theta \approx 38^\circ$, which confirms a disordered structure of the films lacking any long-range periodic arrangement of atoms. On the other hand, the XRD pattern of the annealed film is characterized by the occurrence of several diffraction peaks that can be assigned to the crystalline tetragonal $CuZr_2$ (PDF Card No. 00-018-0466) phase. The thickness of all films investigated was around 2 μ m.

3.2. Non-isothermal crystallization behavior

The non-isothermal crystallization behavior of the amorphous $Zr_{54}Cu_{46}$ and $Zr_{27}Hf_{27}Cu_{46}$ was investigated by differential scanning calorimetry. Both films were heated from room temperature up to 600 °C with a heating rate of 10, 20, 30 and 40 °C/min in pure argon as freestanding film fragments. The non-isothermal crystallization behavior was investigated only for the amorphous films because there was no pronounced response upon heating in case of the crystalline film, as expected.

Fig. 2 shows the most relevant part of DSC curves of both films heated with a heating rate of 30 °C/min. The glass transition temperature T_g , crystallization temperature T_c and the supercooled liquid region $\Delta T = T_c - T_g$ are highlighted on the DSC curves. One can recognize that both films exhibit the glass transition, which gives evidence about their glassy behavior. The substitution of Hf for Zr has nearly no effect on the width of the supercooled liquid region (close to 40 °C for both films) but it shifts the onset of the glass transition and the crystallization to higher temperatures. The enhanced thermal stability of the glassy state of the $Zr_{27}Hf_{27}Cu_{46}$ film compared to the $Zr_{54}Cu_{46}$ film may be explained by a more covalent character of the metallic-covalent bonds of Hf (a higher average bond energy) and also by a lower mobility of Hf during diffusion-controlled processes (approximately twice higher atomic mass of Hf than Zr). Furthermore, the crystallization process of the $Zr_{54}Cu_{46}$ film (Fig. 2a) is characterized by two overlapping exothermic peaks of a higher and lower intensity in contrast to the $Zr_{27}Hf_{27}Cu_{46}$ film (Fig. 2b). These peaks are most likely related to a primary and secondary crystallization (more details given later).

The sets of the crystallization peaks recorded at a heating rate of 10, 20, 30 and 40 °C/min for both films are shown in Fig. 3. The peaks are

Download English Version:

<https://daneshyari.com/en/article/10155579>

Download Persian Version:

<https://daneshyari.com/article/10155579>

[Daneshyari.com](https://daneshyari.com)